communications earth & environment

Article

https://doi.org/10.1038/s43247-024-01406-7

Drought threat to terrestrial gross primary production exacerbated by wildfires

Xuezheng Zong[1,2], Xiaorui Tian[1,2] ✉, Xiaodong Liu[3] & Lifu Shu[1,2]

Frequent droughts have aggravated the occurrence of wildfires and led to substantial losses in terrestrial ecosystems. However, our understanding of compound drought-wildfire events, including the hotspots, spatiotemporal patterns, trends, and their impacts on global vegetation growth, remains unclear. Utilizing satellite data on terrestrial water storage, burned areas, and gross primary production (GPP) from 2002 to 2020, we identified a positive correlation between droughts and wildfires and mapped the global patterns of compound drought-wildfire events. Approximately 38.6% of vegetated areas across the globe witnessed rise in probability of compound drought-wildfire events (< 0.016 events/10a). This increasing trend is spatially asymmetric, and greater amplification is observed across the Northern hemisphere due to frequent droughts. Furthermore, the GPP reductions induced by compound drought-wildfire events are more than twice as high as that caused by isolated droughts. These findings identify hotspots for compound drought-wildfire events and offer quantitative evidence of their greater impacts on ecosystems, aiding in the assessment of compound event risks and the implementation of future climate actions.

Drought is one of the most destructive natural disasters worldwide, affecting society, the environment, and the economy, and can be classified into four types: meteorological (precipitation deficits), hydrologic (abnormally low water levels in lakes, streams, groundwater, and reservoirs), agricultural (decline in soil moisture leading to crop failure), and ecological (episodic water deficits pushing ecosystems beyond vulnerability thresholds)[1–3]. Due to climate change, droughts have become more frequent and intense worldwide in recent decades and are expected to continue through the end of the 21st century[4–7]. Compared with isolated droughts, the wildfires associated with droughts, called as compound drought-wildfire events, can lead to greater adverse impacts on vegetation growth and ecosystem productivity[8,9]. However, there has been little research on the occurrence and hotspots of compound drought-wildfire events at larger scales, as well as their impacts on vegetation growth. Given the pivotal role of terrestrial ecosystems in the global carbon cycle[10,11], a global analysis of compound drought-wildfire events is therefore critical to improve our understanding of compound events impacts on terrestrial ecosystem carbon budget and motivate the implementation of climate actions and wildfire management.

Since the late 1990s, frequent droughts (including compound droughts) have slowed down the increasing trend in global vegetation greenness or even reversed it in some regions[12,13]. Droughts induce the closure of plant stomata, disrupt the water transfer process between plant and soil, result in the demise of individual plants and thus adversely affect ecosystem productivity and carbon sequestration[14–17]. Therefore, past studies have elucidated the detrimental effects of drought on the greenness (e.g., NDVI) and productivity of terrestrial ecosystems, establishing statistical relationships between vapor pressure deficit (VPD)/soil moisture (SM) and vegetation productivity[12,13,18–20]. Remarkably, the occurrence and spread of wildfires are closely linked to dry conditions, with weather-derived and hydrologic variables (e.g., annual or daily flow) exhibiting significant correlations with regional burned areas[21,22]. Fuel stability properties (e.g., fuel distribution, loading, and continuity) show minimal variation over a fire season, but dynamic properties of fuel (moisture content) fluctuate obviously[23]. Dry conditions lead to decreased fuel moisture and increased consumption, and droughts during the fire seasons are often accompanied by high fire danger weather[24–27]. Therefore, droughts often act as a prerequisite for forest fires[28,29]. For instance, in the southeastern Amazon forest, affected by droughts in 2007 and 2010, the total burned area percentages reached 12% and 5%, respectively, markedly surpassing the percentages in normal years ($< 1\%$)[29]. Globally, quantitative studies on the effects of combined drought-wildfire events on vegetation productivity are scarce. Ignoring wildfire occurrences could overlook greater impacts of droughts on vegetation productivity. For example, a study of the spring 2010 drought event in southwestern China reported reductions in gross and net primary ecosystem productivity by 65 and 46 Tg C yr^{-1}, respectively[30]. However, this study overlooked the severe wildfires during this period, which showed a

[1]Ecology and Nature Conservation Institute, Chinese Academy of Forestry, Beijing, China. [2]Key Laboratory of Forest Protection of National Forestry and Grassland Administration, Beijing, China. [3]School of Ecology and Nature Conservation, Beijing Forestry University, Beijing, China. ✉e-mail: tianxr@caf.ac.cn

higher frequency and larger burned areas compared to other seasons[31,32]. Similarly, a recent study underscored the adverse effects of warmer and drier conditions on vegetation in the southwest China in 2022 but also neglected the influence of wildfires[33]. The substantial reductions in vegetation productivity in this region were evidently influenced by the wildfire events induced by droughts. A 2019–2020 survey of Australian fires found that ecosystems solely affected by drought swiftly recovered with abundant February precipitation and favorable temperatures in 2020, whereas those impacted by fire have yet to recover[34]. This study further emphasizes the greater impacts of combined drought-wildfire events on ecosystems.

To this end, we conduct a global analysis of spatiotemporal patterns of compound drought-wildfire events and analyze their impacts on global vegetation gross primary production (GPP) by using remotely sensed Terrestrial Water Storage Anomalies (TWSA), wildfire, and GPP data. Specifically, we aim to address the following two questions: (1) what spatiotemporal patterns of compound drought-wildfire events, and where are their hotspot regions during the period of 2002 to 2020? (2) How magnitude in impacts of compound drought-wildfire events on GPP compared with isolated droughts? Answering these two questions are important because they can provide initial guidance of where regions need to be implemented urgently for climate actions.

Results

Hotspots of compound drought-wildfire events

The Likelihood Multiplication Factor (LMF) is a metric designed to clarify the impact of independent drought and wildfire event probabilities on their joint occurrence probability. An LMF greater than 1 indicates a strong correlation between droughts and wildfires, suggesting that drought occurrences increase wildfire events to some extent, thus promoting the occurrence of compound drought-wildfire events at spatiotemporal scales. In the past two decades, obvious geographical variations in the global occurrence of compound drought-wildfire events have been observed (Fig. 1). Specifically, South Africa shows the highest probability of compound drought-wildfire events, with an average probability of 0.1. This probability corresponds to an annual occurrence of drought-wildfire composite events, with a return period of 0.8 year. Furthermore, regions with return periods of less than 1 year (probabilities exceeding 0.08) also include Eastern Europe, Northwestern and Southern Asia, Central and Southern North America, Eastern South America, and Eastern Oceania (Australia). This suggests a high probability of compound drought-wildfire events in these areas, indicating the susceptibility of ecosystems to this compound event.

Annually, we employed trend analysis (MK test) to examine the probability trend of compound drought-wildfire events during the study period, offering deeper insights into hotspot regions for compound events (CEs) occurrences. The results indicate approximately 38.6% of the world's vegetated pixels exhibited an increased probability of compound drought-wildfire events from 2002 to 2020 (Fig. 2). These findings reveal spatial asymmetry, with a significant portion (68.7%) of Europe's vegetated areas experiencing more frequent compound drought-wildfire events compared to other regions, attributed to escalating droughts within the period. The regions following are Asia, South America, North America, Australia, and Africa, with the percentages of vegetated pixels showing an increased probability of compound drought-wildfire events being 43%, 41.7%, 39.9%, 20.2%, and 18.7%, respectively. Notably, pixels showing a significant increase ($P < 0.05$) are predominantly located in Eastern Europe, Southern and Northeastern Asia, Central and Southern North America, Eastern South America, and Eastern Oceania (Australia), with increase rates of 0.01–0.016 event per decade.

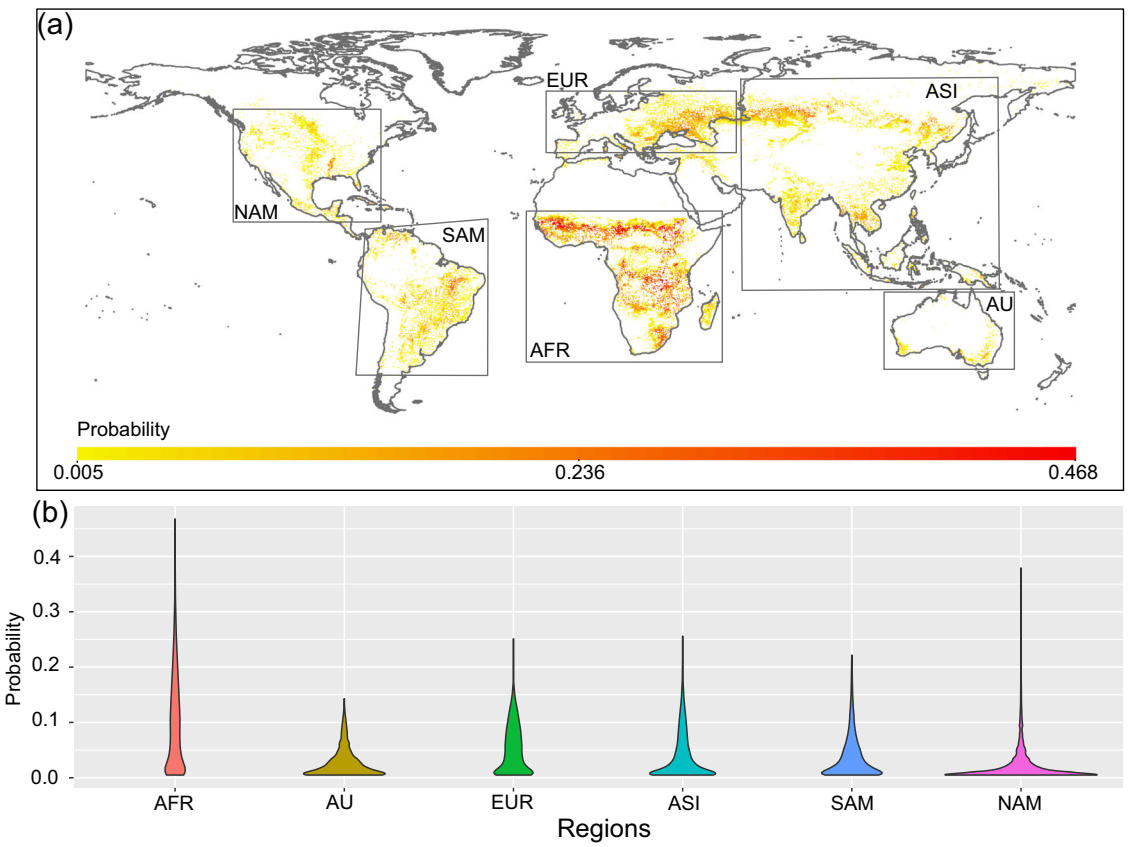

Fig. 1 | Hotspots of compound drought-wildfire events. a is the spatial distribution of compound drought-wildfire events. Higher probability indicate the compound drought-wildfire events occurred frequently over the study period. **b** represents the average probability of compound drought-wildfire events, which is calculated by pixels experienced compound events during the study period. AFR, AU, EUR, ASI, SAM, and NAM are abbreviations of Africa, Australia, Europe, Asia, South America, and North America, respectively.

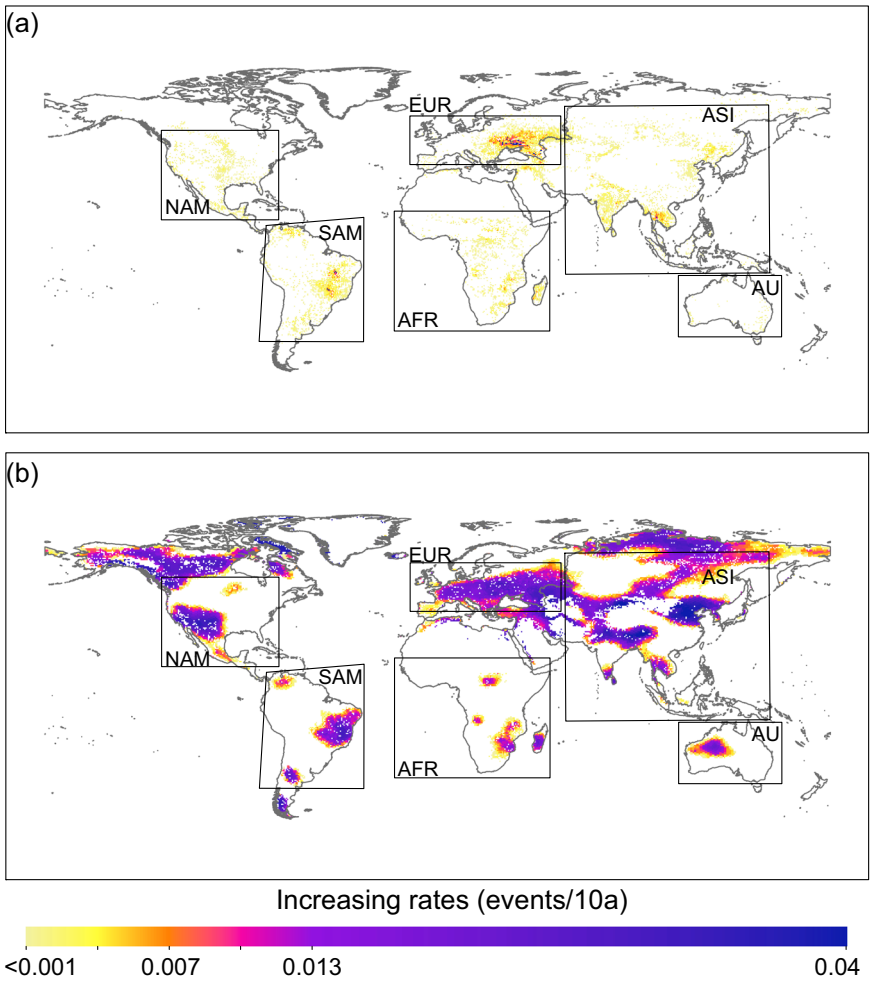

Fig. 2 | Spatial patterns of increasing trends in the probability of compound drought-wildfire events and droughts. a presents the spatial distribution of pixels with increasing trends in probability of compound drought-wildfire events over the period of 2002–2020. **b** is the spatial distribution of pixels with increasing trends in probability of droughts over the period. A significance level ($\alpha = 0.05$) is used to detect the increasing trend during the period.

Probabilities of each vegetation type experienced compound events

Significant variation in the probability of compound drought-wildfire events was noted among different vegetation types (Fig. 3). In Africa, grasslands and savannas (tree cover 10–30% with canopy >2 m) are the two primary vegetation types for compound drought-wildfire events, accounting for 51.9% and 24.2% of all vegetated pixels, respectively. Both vegetation types displayed a high probability of such compound events, with probabilities of 0.1 (return period <1 year) throughout the study period. Additionally, croplands (at least 60% of the area cultivated cropland), mixed forests (dominated by neither deciduous nor evergreen tree type (40–60% of each) with canopy >2 m), and Cropland/Natural Vegetation Mosaics (mosaics of small-scale cultivation 40–60% with natural tree, shrub, or herbaceous vegetation) also showed a higher probability (> 0.08) of the compound drought-wildfire events.

The probability of compound drought-wildfire events for all vegetation types in other geographic regions remained below 0.08. In terms of vegetation type distribution, compound drought-wildfire events in Europe predominantly occurred in croplands, grasslands, and mixed forests, constituting 56%, 16.7%, and 14.3% of cases, respectively. The average occurrence probability for these vegetation types varied from 0.02 to 0.07. In North America, Asia, and Eastern Oceania, over 30% of compound drought-wildfire events were recorded in croplands and grasslands. In South America, beyond grasslands and savannas, evergreen broadleaf forests, which experienced compound drought-wildfire events (characterized by evergreen broadleaf and palmate trees with a canopy >2 m and tree cover >60%), accounted for a significant proportion of 16.7%.

Seasonal patterns of compound drought-wildfire events in different regions

Globally, the probability of compound drought-wildfire events and their spatial distribution show significant monthly variations, closely tied to the local climate (Fig. 4). In the Northern Hemisphere, compound drought-wildfire events typically occur from March to October, covering spring, summer, and autumn. For instance, in Northern Asia and Central and Southern North America, the average probability of compound drought-wildfire events in spring (March–May) is 0.01, peaking in May at 0.016 and 0.011, respectively. In winter (December-January), compound drought-wildfire events mainly occur in Southern Asia, with an average probability of less than 0.01. In Eastern Europe, the highest probability of compound drought-wildfire events is observed in August (0.17), significantly higher than in other months. These events can exacerbate wildfire risk, leading to ecological and economic losses in vital agricultural and forested areas across many Northern Hemisphere countries.

In the Southern Hemisphere, northern Africa experiences compound drought-wildfire events primarily in January-March and November-December, with average probabilities ranging from 0.017 to 0.028 and 0.017 to 0.021, respectively, peaking in January at 0.028. Southern Africa is susceptible to these compound events in June-September (winter), with average probabilities ranging from 0.019 to 0.024. In Eastern Oceania, particularly in Southwestern and Southeastern Australia, the probability of compound drought-wildfire events is higher in April and May, at 0.015 and 0.013, respectively, compared to 0.005–0.008 in other months.

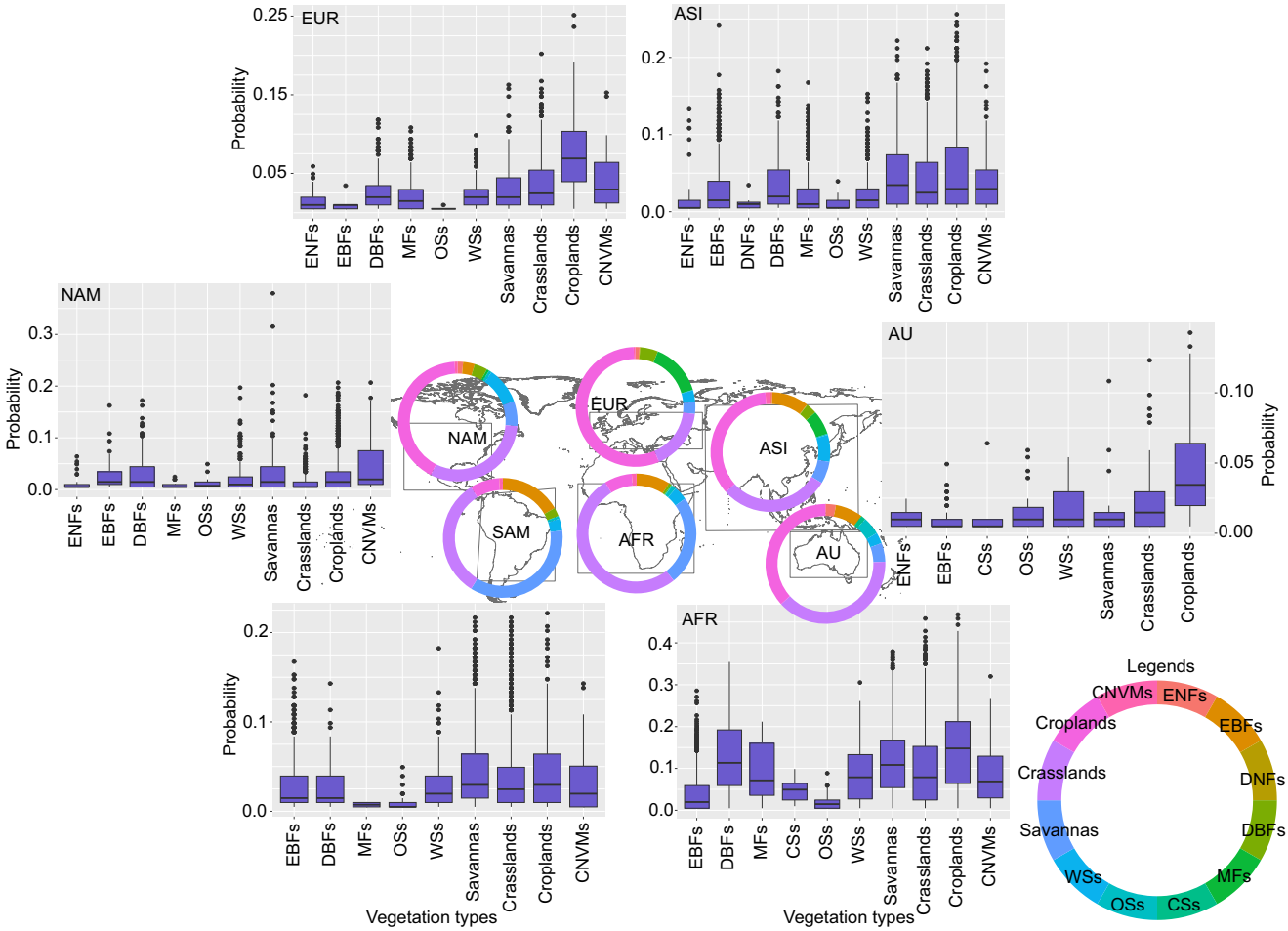

Fig. 3 | Percentages of each vegetation type experienced compound drought-wildfire events and their probabilities across different regions over the study period. The donut chart is the percentages of compound drought-wildfire events in different vegetation types across six regions. The boxplot of each region is mapped based on pixels experienced compound events over the period. ENFs, EBFs, DNFs, DBFs, MFs, CSs, OSs, WSs, and CNVMs are abbreviations of evergreen needleleaf forests, evergreen broadleaf forests, deciduous needleleaf forests, deciduous broadleaf forests, mixed forests, closed shrublands, open shrublands, woody savannas, and cropland/natural vegetation mosaics, respectively.

Impacts of compound drought-wildfire events on GPP

We used a bottom-up approach to compile datasets Of Gross Primary Production (GPP) losses due to drought and compound drought-wildfire events, respectively. Following this, we spatially mapped the resistance of GPP and its losses to these events. Our findings suggest that during compound drought-wildfire events, every vegetation type demonstrates notably weaker resistance compared to isolated drought events (Fig. 5). This suggests that compound drought-wildfire events are more likely to reduce GPP than droughts in a specific region.

The GPP reductions from compound drought-wildfire events were significantly greater than those caused by drought events across all vegetation types and geographic regions (Fig. 6). This observation emphasizes that compound drought-wildfire events have more pronounced and harmful effects on GPP, making vegetation less resilient than to isolated drought. For instance, in Europe, the average GPP reduction due to compound drought-wildfire events was 18.2%, significantly surpassing the impact of isolated droughts, which was 8.4%.

The GPP reduction due to compound drought-wildfire events also varies across different vegetation types. Generally, compound drought-wildfire events cause more severe GPP losses in grasslands, croplands, savannas, and Cropland/Natural Vegetation Mosaics than in forested vegetation types within the same geographical regions, especially in Europe and North America. This observation suggests that compound drought-wildfire events are more likely to adversely affect agricultural production in these regions. The adverse impacts of compound drought-wildfire events are also greater in deciduous coniferous forests and deciduous broadleaf forests in Asia, with GPP reductions between 28% and 35%. Moreover, the detrimental impacts of compound drought-wildfire events on shrubland are more severe in Africa, South America, and Australia, with GPP reductions ranging from 20% to 30%.

Discussion

In recent decades, multiple hazards or drivers frequently occur simultaneously or sequentially, forming compound events (CEs)[35,36] that lead to or amplify negative impacts on ecosystems compared to a single hazard[37,38]. Consequently, the study of compound events has attracted increased attention[9,39,40]. Recent research has explored the interactions between meteorological droughts and extreme wildfire risk, analyzing spatio-temporal patterns of their co-occurrence, and predicting future trends under climate change[24–27]. For instance, Ridder et al.[25] noted a higher probability of compound meteorological drought-high wildfire weather events during spring and summer in the Northern Hemisphere, which could exacerbate wildfire risks and economic losses in vital agricultural regions in North America and Europe. Our study also identifies these regions as hotspots for compound drought-wildfire events over the past two decades.

We discovered that the probability of compound drought-wildfire events has substantially increased in certain areas since 2002, often due to

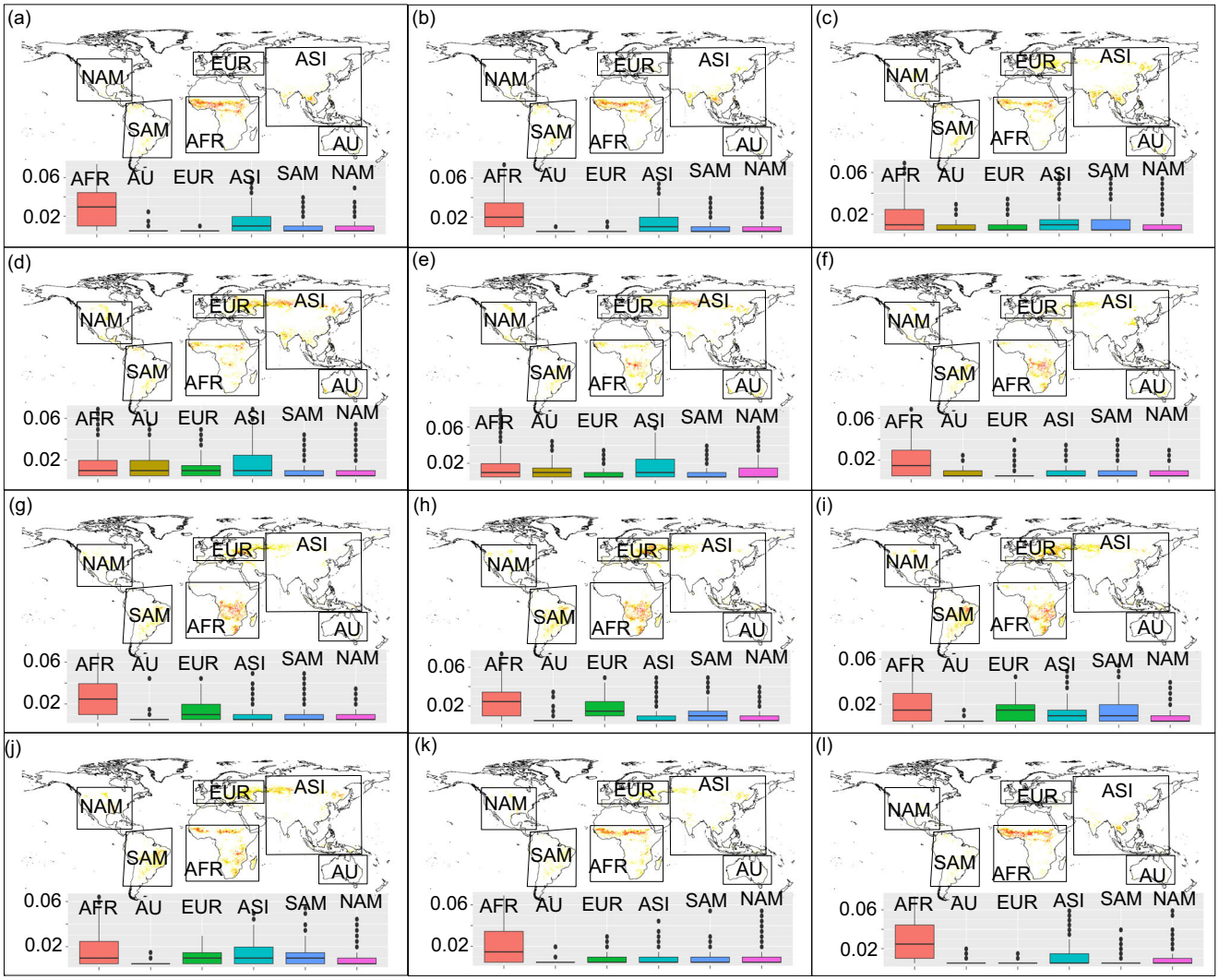

Fig. 4 | Monthly probability of compound drought-wildfire events in six major regions. This figure illustrates the occurrence of compound drought-wildfire events in six regions at month scale. **a**–**l** are January, February, March, April, May, June, July, August, September, October, November, and December, respectively.

more frequent droughts[41–43]. Over longer timescales, climate significantly influences the amounts and types of fuel[44,45]. On shorter timescales (hourly to monthly), weather factors such as temperature, precipitation, winds, and atmospheric humidity strongly correlate with fire activity in a region, especially during extreme wildfire years[46,47]. Recent global wildfire cases underscored that weather factors are key drivers of inter-annual variability in wildfire activity[9,47], with their occurrence and spread influenced by preceding dry weather conditions. For example, in summer 2022, the unprecedented and prolonged co-occurrence of heatwaves and droughts led to frequent and intense wildfires in Chongqing, China[48]. Importantly, forest fire management practices also influence the process of fire occurrence and spread. The skewed distribution of burned areas closely relates to the effectiveness of firefighting efforts, where a high initial suppression success rate significantly limits the size of wildfires under high-risk weather conditions[49]. Thus, analyzing the occurrence patterns of drought-wildfire events offers a comprehensive understanding of the interactions among droughts, wildfires, and fire management across extensive spatial and temporal scales. This analysis is invaluable for developing future climate change scenarios and establishing a foundation for adaptation strategies in forest and fire management.

Although the outbreak of coronavirus disease 2019 (COVID-19) significantly altered wildfire occurrences[50–52] and had a positive impact on vegetation greenness and GPP in most world regions[53–55], the adverse effects of drought, especially compound drought-wildfire events on vegetation growth and GPP, have consistently captured worldwide attention in recent years. Due to land-atmosphere feedback, increased atmospheric water demand leads to further soil water content depletion, creating a positive feedback loop that significantly impacts vegetation beyond the effects of a single event alone[13,56]. Water stress leads to a decrease in leaf stomatal conductance to reduce water consumption, causing a concurrent reduction in CO_2 uptake by plants. The combined effects of water stress and carbon reduction, linked to extremely low soil moisture (SM) and high vapor pressure deficit (VPD), have considerably negative impacts on vegetation growth[57,58]. Moreover, dry conditions enhance evapotranspiration and reduce fuel moisture, leading to increased fuel combustion[59] and causing intense fire behavior[60]. Therefore, intense wildfires can further exacerbate drought's negative impacts on vegetation. For example, a study indicated that the aboveground biomass (AGB) in forest areas affected by compound drought-wildfire events in Australia decreased by 0.17 Pg C during 2019–2020, more than five times the AGB loss (0.03 Pg C) in areas affected by drought alone[61]. Although some studies have explored the relationship between wildfires, drought, and the global carbon cycle[13,62], quantitative analyses of compound drought-wildfire events and their impacts remain limited. Recent studies have also revealed significant time-lag effects in vegetation responses to extreme climate events (e.g., droughts)[63,64]. These studies recognize the vegetation growth may primarily be also driven by the

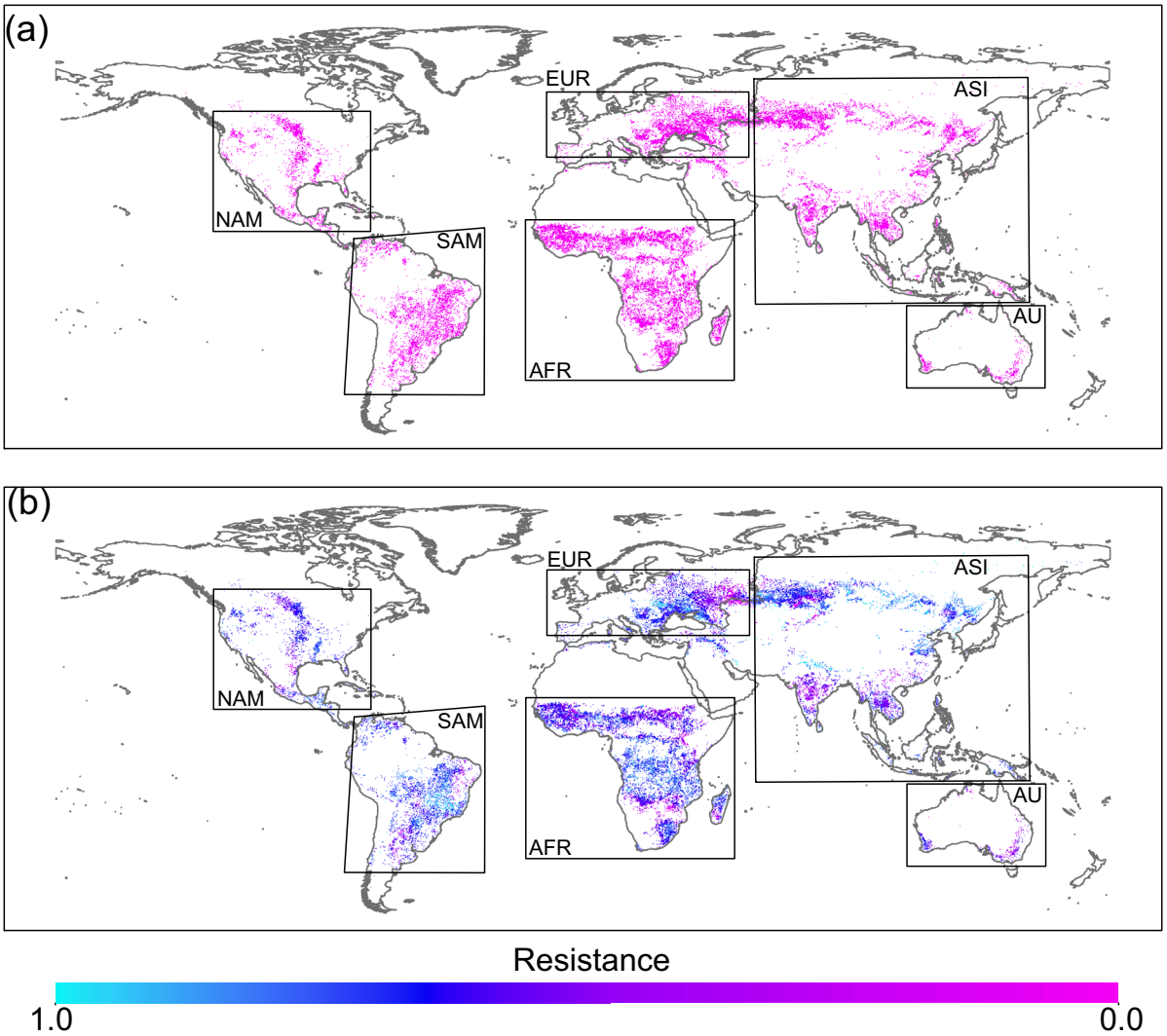

Fig. 5 | Spatial patterns of GPP resistance to drought and compound drought-wildfire events. a GPP resistance to compound drought-wildfire events (**b**) GPP resistance to droughts. The greater GPP loss of an ecosystem during compound events indicates lower resistance.

earlier climatic conditions (not including the current month). Therefore, studying the time-lag effects in vegetation responses to compound events should be considered in follow-up work. In summary, our findings highlight the importance of compound drought-wildfire events in affecting GPP and offer a deeper understanding of how vegetation production responds directly to such events. The results can also form the basis for enhancing wildfire management through drought prediction and monitoring information.

We primarily used terrestrial water storage data, MODIS wildfire product data, and vegetation GPP data to analyze the global pattern of compound drought-wildfire events and their impact on vegetation growth over the past two decades. We selected several globally representative cases of compound drought-wildfire events to improve research accuracy (Fig. 7). Importantly, identifying hotspots for compound events highlights key regions for future research on compound drought-wildfire events. Considering the resolution limitations and partial absence of terrestrial water storage data, we recommend using other observations and remotely sensed data with higher accuracy for future research, especially in hotspot areas. Furthermore, this study adopted a bottom-up approach to accurately explore the impacts of compound drought-wildfire events on vegetation, primarily focusing on the co-occurrence of drought and wildfires to form a multivariate event. It's essential to note that types of compound events include three other categories: temporal, spatial, and preconditioning, each of which can also significantly impact ecosystems and socioeconomics[65]. For example, the forest fires in the Amazon in 2018 were associated with a pre-existing and persistent drought[66], indicating sequential continuity over time. In conclusion, our study highlights the spatial and temporal patterns of compound events formed by the co-occurrence of drought and wildfires, underscoring the severity of their impacts on vegetation. This sets the foundation for future correlation analyses involving other types of composite events related to droughts and wildfires, utilizing appropriate data.

Methods

Data and preprocess

The global vegetation classification data were obtained using the MODIS-MCD12Q1 Global Land Cover Product (2002–2020) (available at https://lpdaac.usgs.gov/products/mcd12q1v006/). This product is based on the International Geosphere-Biosphere Programme (IGBP) classification, delineating 17 land cover types. The land cover product was first processed as follows:

(1) For each pixel, time series data for land cover types were established using annual land cover data.
(2) Pixels consistently classified as non-vegetation types (permanent wetlands, urban and built-up lands, permanent snow and ice, barren, and water bodies) were excluded.

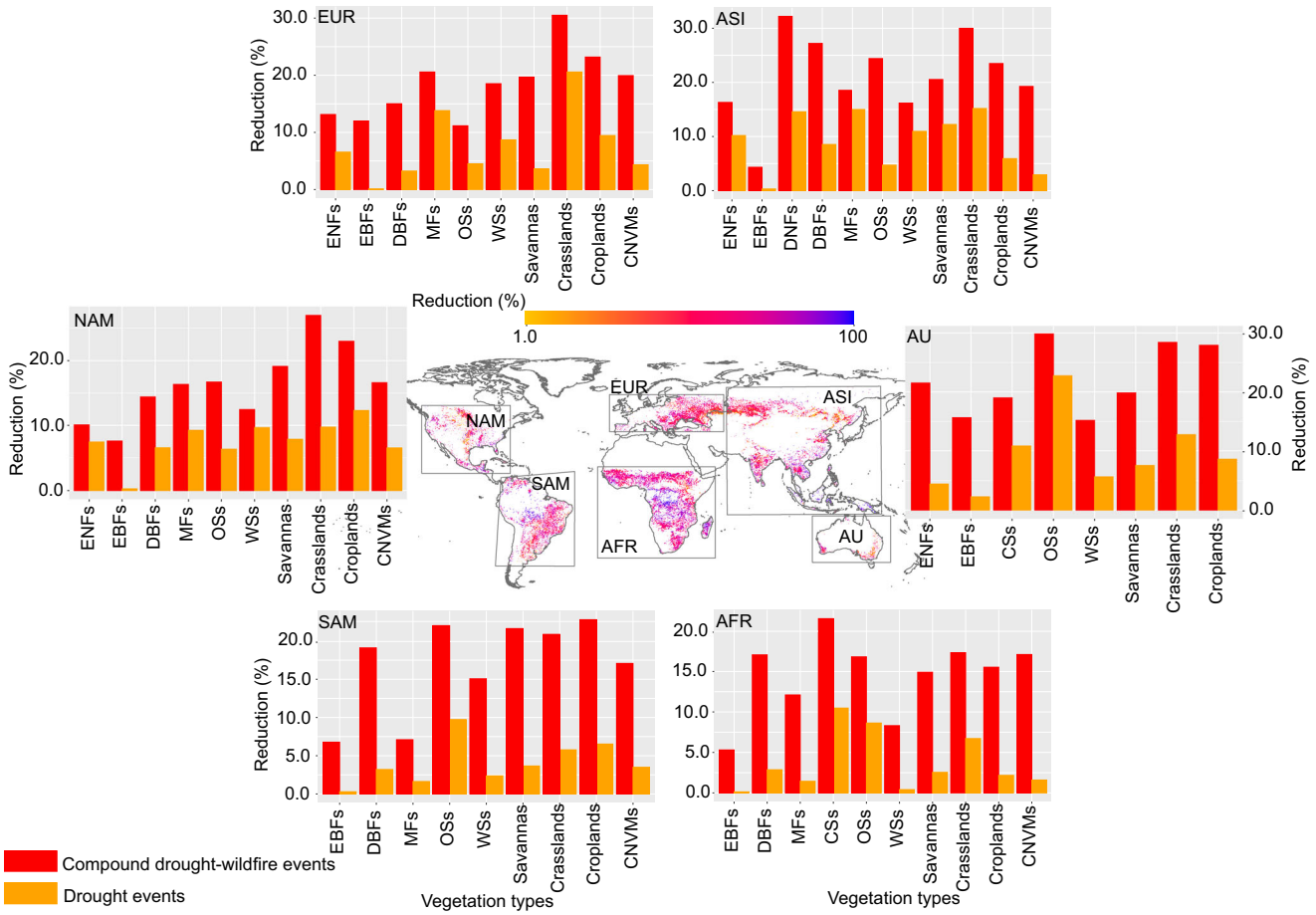

Fig. 6 | GPP reductions (%) after compound events across different regions and vegetation types. The GPP reduction due to compound drought-wildfire events in each pixel was calculated as the difference of the GPP value of the months of compound drought-wildfire events and the normal conditions. Average GPP reductions for each vegetation type are showed by bar plots through the spatial integration of GPP reduction pixel by pixel.

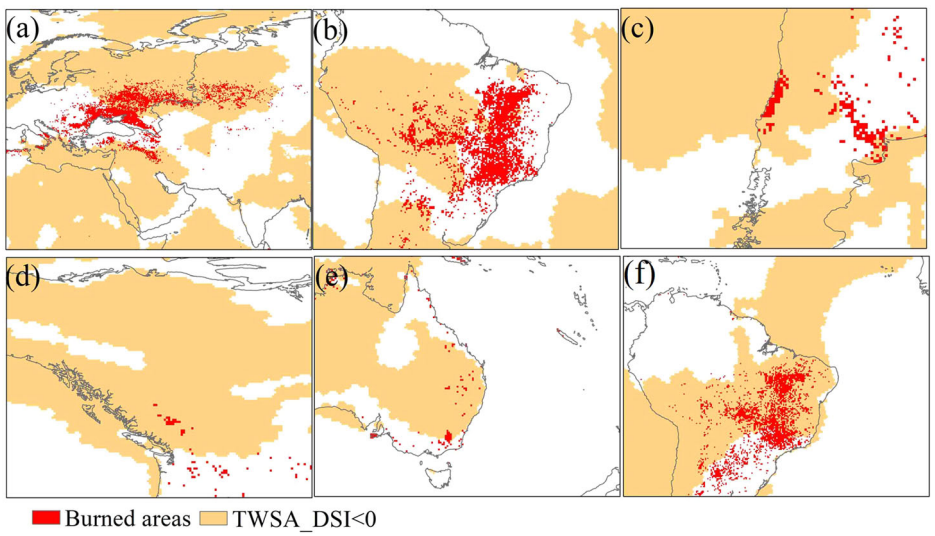

Fig. 7 | Six cases of compound drought-wildfire events. a wildfires in Russia and Europe in 2010; **b** wildfires in Amazon Rain Forest in 2010; **c** Wildfires in Chile in 2017; **d** wildfires in USA in 2017; **e** Australia wildfires during 2019/2020 fire season; **f** wildfires in Brazil in 2020.

(3) Considering frequent wildfires can cause vegetation damage and lead to changes in vegetation type, any vegetated pixels with significant vegetation type changes (e.g., from tree cover to urban fabric) across continuous years without recorded wildfires were excluded.
(4) Any remaining pixels consistent in vegetation types throughout the study period were retained.

This approach aims to exclude the influence of changes in vegetation types on the results, considering factors such as human activities. The 12 classified vegetation types are as follows: evergreen coniferous forests (ENFs), evergreen broadleaf forests (EBFs), deciduous coniferous forests (DNFs), deciduous broadleaf forests (DBFs), mixed forests (MFs), Closed Shrublands (CSs), Open Shrublands (OSs), Wooded Grasslands (WSs),

Savannas, Grasslands (WG), Croplands, and Cropland/Natural Vegetation Mosaics (CNVMs).

The global GPP dataset for the period 2002–2020 (0.05 × 0.05° spatial resolutions, 8-day temporal resolutions) were downloaded from Bi et al. (2022). This dataset was produced by using an updated two-leaf light use efficiency model (TL-LUE), which is driven by the GLOBMAP leaf area index, CRUJRA meteorology, and ESA-CCI land cover[67]. In addition to their good performance in the estimation of GPP for all vegetation types, the dataset advances our in-depth understanding of large-scale carbon cycle processes and dynamics.

The burned area (BA) data for the period 2002–2020 were acquired from the MODIS-MCD64A1 product (https://ladsweb.modaps.eosdis.nasa.gov/search/). This dataset has a spatial resolution of 500 m and has been categorized into monthly statistics which classifies each pixel as burned (with indication of the estimated day of burning), unburned, or unmapped if insufficient data were available to determine the burnt/unburned status[68,69]. To enhance data accuracy, false burned areas—characterized as redundant information outside of vegetation areas—were eliminated from the MODIS-MCD64A1 product based on vegetation distribution. Subsequently, the processed monthly burned area data were resampled to a 0.05° resolution using nearest neighbor interpolation to facilitate data handling and enhance pattern recognition[68,70].

Satellite gravity data were employed to invert monthly-scale total terrestrial water availability, serving as an aggregate indicator of overall regional drought conditions in recent years[6,71]. This study collected mass concentration blocks (Mascons; M) from three sources: Space Research at Texas State University (CSR), Jet Propulsion Laboratory (JPL), and NASA Goddard Space Flight Center (GSFC). In this study, a weighted average method was used to derive the Total Terrestrial Water Storage Anomaly (TWSA) monthly dataset covering the globe from 2002 to 2020, comprising a total of 203 months of data, with the remainder unprocessed due to missing measurements from instrument issues. The TWSA Drought Severity Index (TWSA_DSI) was used to indicate droughts[71]. This index is a dimensionless standardized water storage anomaly index, effectively indicating the degree of drought occurrence and its spatial variability across different geographic regions. Equation (1) was utilized to calculate the TWSA_DSI dataset for each month throughout the study period.

$$\mathrm{TWSA\_DSI}_{i,j} = \frac{(\mathrm{TWSA}_{i,j} - \overline{\mathrm{TWSA}_j})}{\sigma_j} \quad (1)$$

Where $\mathrm{TWSA}_{i,j}$ represents the TWSA data for month j of year i. TWSA_DSI and σ are the mean and standard deviation of TWSA for month j of the study period, respectively; $\overline{\mathrm{TWSA}_j}$ and σ_j are the mean and standard deviation of TWSA for month j of the study period, respectively. A negative value of TWSA_DSI indicates that the total land water availability is lower than the historical average, and a larger absolute value indicates a more severe drought.

Definition of compound events

Compound events[65] are defined as the simultaneous occurrence of drought and wildfires within the same month in a given region. For each pixel a, if it experiences drought ($\mathrm{TWSA\_DSI}_i < 0$) and wildfire ($\mathrm{BA}_i > 0$) on the same month i (from 1 to 12), it is categorized as a compound drought-wildfire events (Eq. 2).

$$\mathrm{CEs}_i = \begin{cases} 1, & \mathrm{TWSA\_DSI}_i < 0 \text{ and } \mathrm{BA}_i > 0 \\ 0, & \text{otherwise} \end{cases} \quad (2)$$

The probability (P_{actual}) of compound drought-wildfire events is defined as the ratio of the number of months on which the CEs occur ($\sum_{i=1}^{n}\mathrm{Months}(\mathrm{CEs}=1)_i$) to the total number of months in the study period ($P_{\mathrm{actual}} = \frac{\sum_{i=1}^{n}\mathrm{Months}(\mathrm{MEs}=1)_i}{203}$). Then, the return period (yrs) is calculated from the inverse relationship between the probability and recurrence period ($RP = \frac{1}{P_{\mathrm{actual}} \times 12}$)[25]. Theoretically, when the occurrence of drought and wildfire are independent events, the probability of co-occurrence of compound drought-wildfire events (P_{indep}) can be expressed by the product of their respective probabilities of occurrence, i.e.,:

$$P_{\mathrm{indep}} = \frac{\sum_{i=1}^{n}\mathrm{Months}(\mathrm{droughts})_i}{203} \times \frac{\sum_{i=1}^{n}\mathrm{Months}(\mathrm{fires})_i}{203} \quad (3)$$

Therefore, we test the correlation between these two events by the ratio of the actual probability (P_{actual}) and the theoretical probability (P_{indep}) of the compound drought-wildfire events, namely Likelihood multiplication factor (LMF))[59]. Accordingly: (1) LMF equals 1, which means that the drought and wildfire are independent of each other; (2) LMF > 1, means that there is a positive correlation between drought and wildfire; and (3) LMF < 1, means that there is a negative correlation between the events of drought and wildfire[25].

Response of GPP to compound drought-wildfire events

Vegetation resistance to extreme events is the ability of vegetation to maintain its structure and function despite extreme disturbances[72,73], that is, the vegetation index remains stable or is not negatively impacted by such events[74,75]. Based on this definition, the probability of negative vegetation GPP anomalies occurring simultaneously within each image element during compound drought-wildfire events was calculated and denoted as $F_{\mathrm{com\_ano}}$[76]. Combined with the probability of occurrence of the compound drought-wildfire event (P_{actual}), the resistance of vegetation to the compound event (R_s) can be calculated:

$$R_s = 1 - \frac{F_{\mathrm{com\_ano}}}{P_{\mathrm{actual}}} \quad (4)$$

Where R_s indicates the resistance of vegetation, which ranges from 0 to1. The lower the value indicates that $F_{\mathrm{com\_ano}}$ is closer to P_{actual}, that is, the vegetation resistance to the compound drought-wildfire events is lower, and the GPP decreases during the compound event. When R_s equals 1, it indicates that the occurrence probability of $F_{\mathrm{com\_ano}}$ is closer to zero, which means the vegetation has strong resistance to the compound drought-wildfire events.

The ratio of the vegetation growth index during the disturbance period to the vegetation index under normal conditions indicates the extent of the event's impact and the vegetation's resilience[76–78]. Accordingly, taking the average GPP values in normal months as the baseline, the reduction in GPP due to compound drought-wildfire events for each pixel was calculated as the difference between the GPP of the months of compound events and the baseline[79]:

$$R_i = \frac{\mathrm{Veg}_{\mathrm{normal}} - \mathrm{Veg}_{\mathrm{com}}}{\mathrm{Veg}_{\mathrm{normal}}} \times 100\% \quad (5)$$

where $\mathrm{Veg}_{\mathrm{com}}$ denotes the GPP during the duration phase of the compound drought-wildfire events, and $\mathrm{Veg}_{\mathrm{normal}}$ is the mean value of the vegetation index under normal weather conditions at the corresponding time period. $R_i > 0$ indicates that the compound drought-wildfire events reduced the vegetation GPP, and a larger value indicates a more severe loss of GPP. This index is a dimensionless standardized GPP reduction anomaly index and can effectively indicates the impacts of compound drought-wildfire events on GPP and shows spatial variability across different geographic regions. Additionally, we estimated the GPP reductions across different vegetation types in each terrestrial ecosystem due to the compound drought-wildfire events.

Data availability

Burned area data for the 2002–2020 period were obtained from the MODIS-MCD64A1 product (https://ladsweb.modaps.eosdis.nasa.gov/search/order/1/MCD64A1--61). Global vegetation classification data were sourced from

the MODIS-MCD12Q1 Global Land Cover Product (2002–2020) (https://ladsweb.modaps.eosdis.nasa.gov/search/order/1/MCD12Q1--61). The global 0.05° dataset for GPP (1992–2020) were acquired through the Zenodo service (https://zenodo.org/records/6518002). Three GRACE products used in this study can be obtained from CSR_Mascon (https://www2.csr.utexas.edu/grace/RL06_mascons.html), JPL_Mascon (https://grace.jpl.nasa.gov/data/get-data/jpl_global_mascons/), and GSFC_Mascon (https://earth.gsfc.nasa.gov/geo/data/grace-mascons).

Code availability

Post-processing R scripts for metric computation, bootstrapping, and jitter plots are available from the corresponding author on reasonable request.

Received: 11 December 2023; Accepted: 19 April 2024;
Published online: 29 April 2024

References

1. Zargar, A., Sadiq, R., Naser, B. & Khan, F. I. A review of drought indices. *Environ. Rev.* **19**, 333–349 (2011).
2. Apurv, T., Sivapalan, M. & Cai, X. Understanding the role of climate characteristics in drought propagation. *Water Resour. Res.* **53**, 9304–9329 (2017).
3. Crausbay, S. D. et al. Defining ecological drought for the twenty-first century. *B. Am. Meteorol. Soc.* **98**, 2543–2550 (2017).
4. Vicente-Serrano, S. M. et al. Global drought trends and future projections. *Philos. T. R. Soc. A.* **380**, 20210285 (2022).
5. Christian, J. I. et al. Global distribution, trends, and drivers of flash drought occurrence. *Nat. Commun.* **12**, 6330 (2021).
6. Pokhrel, Y. et al. Global terrestrial water storage and drought severity under climate change. *Nat. Clim. Change* **11**, 226–233 (2021).
7. Xu, L., Chen, N. & Zhang, X. Global drought trends under 1.5 and 2 °C warming. *Int. J. Climatol.* **39**, 2375–2385 (2019).
8. Boer, M. M., Resco de Dios, V. & Bradstock, R. A. Unprecedented burn area of Australian mega forest fires. *Nat. Clim. Change* **10**, 171–172 (2020).
9. White, R. H. et al. The unprecedented Pacific Northwest heatwave of June 2021. *Nat. Commun.* **14**, 727 (2023).
10. Anav, A. et al. Spatiotemporal patterns of terrestrial gross primary production: a review. *Rev. Geophys.* **53**, 785–818 (2015).
11. Campbell, J. E. et al. Large historical growth in global terrestrial gross primary production. *Nature* **544**, 84–87 (2017).
12. Feng, X. et al. Recent leveling off of vegetation greenness and primary production reveals the increasing soil water limitations on the greening Earth. *Sci. Bull.* **66**, 1462–1471 (2021).
13. Liu, X. et al. Compound droughts slow down the greening of the Earth. *Global Change Biol.* **29**, 3072–3084 (2023).
14. De Boeck, H. J. & Verbeeck, H. Drought-associated changes in climate and their relevance for ecosystem experiments and models. *Biogeosciences* **8**, 1121–1130 (2011).
15. Grimm, N. B. et al. Climate-change impacts on ecological systems: introduction to a US assessment. *Front. Ecol. Environ.* **11**, 456–464 (2013).
16. Reichstein, M. et al. Climate extremes and the carbon cycle. *Nature* **500**, 287–295 (2013).
17. Doughty, C. E. et al. Drought impact on forest carbon dynamics and fluxes in Amazonia. *Nature* **519**, 78–82 (2015).
18. Yuan, W. et al. Increased atmospheric vapor pressure deficit reduces global vegetation growth. *Sci. Adv.* **5**, eaax1396 (2019).
19. Liu, L. et al. Soil moisture dominates dryness stress on ecosystem production globally. *Nat. Commun.* **11**, 4892 (2020).
20. Fu, Z. et al. Atmospheric dryness reduces photosynthesis along a large range of soil water deficits. *Nat. Commun.* **13**, 989 (2022).
21. Chan, X. Y. et al. Assessment of lake-level fluctuation as an indicator of fire activity in boreal Canada. *Ecol. Indic.* **145**, 109611 (2022).
22. Bowman, D. M. J. S. et al. Vegetation fires in the Anthropocene. *Nat. Rev. Earth Env.* **1**, 500–515 (2020).
23. Ellis, T. M., Bowman, D. M. J. S., Jain, P., Flannigan, M. D. & Williamson, G. J. Global increase in wildfire risk due to climate-driven declines in fuel moisture. *Global Change Biol.* **28**, 1544–1559 (2022).
24. Richardson, D. et al. Global increase in wildfire potential from compound fire weather and drought. *NPJ Clim. Atmos. Sci.* **5**, 23 (2022).
25. Ridder, N. N. et al. Global hotspots for the occurrence of compound events. *Nat. Commun.* **11**, 5956 (2020).
26. Ridder, N. N., Ukkola, A. M., Pitman, A. J. & Perkins-Kirkpatrick, S. E. Increased occurrence of high impact compound events under climate change. *NPJ Clim. Atmos. Sci.* **5**, 3 (2022).
27. Fan, X. et al. Escalating hot-dry extremes amplify compound fire weather risk. *Earth's Future* **11**, e2023EF003976 (2023).
28. Forkel, M. et al. Extreme fire events are related to previous-year surface moisture conditions in permafrost-underlain larch forests of Siberia. *Environ. Res. Lett.* **7**, 044021 (2012).
29. Brando, P. M. et al. Abrupt increases in Amazonian tree mortality due to drought–fire interactions. *Proc. Natl Acad. Sci. USA* **111**, 6347–6352 (2014).
30. Zhang, L. et al. The 2010 spring drought reduced primary productivity in southwestern China. *Environ. Res. Lett.* **7**, 045706 (2012).
31. Wang, W., Zhao, F., Wang, Y., Huang, X. & Ye, J. Seasonal differences in the spatial patterns of wildfire drivers and susceptibility in the southwest mountains of China. *Sci. Total Environ.* **869**, 161782 (2023).
32. Ying, L. et al. Relative humidity and agricultural activities dominate wildfire ignitions in Yunnan, Southwest China: Patterns, thresholds, and implications. *Agr. Forest Meteorol.* **307**, 108540 (2021).
33. Xu, W. et al. Impacts of record-breaking compound heatwave and drought events in 2022 China on vegetation growth. *Agr. Forest Meteorol.* **344**, 109799 (2024).
34. Byrne, B. et al. The carbon cycle of Southeast Australia during 2019–2020: drought, fires, and subsequent recovery. *AGU Adv.* **2**, e2021AV000469 (2021).
35. Seneviratne, S. I. et al. in *Climate Change 2021: The Physical Science Basis. Contribution of Working Group I to the Sixth Assessment Report of the Intergovernmental Panel on Climate Change* (eds Masson-Delmotte, V. et al.) 1513–1766 (Cambridge University Press, 2021).
36. Zscheischler, J. & Lehner, F. Attributing compound events to anthropogenic climate change. *B. Am. Meteorol. Soc.* **103**, E936–E953 (2022).
37. Kemter, M. et al. Cascading hazards in the aftermath of Australia's 2019/2020 Black Summer Wildfires. *Earth's Future* **9**, e2020EF001884 (2021).
38. Taufik, M. et al. Amplification of wildfire area burnt by hydrological drought in the humid tropics. *Nat. Clim. Change* **7**, 428–431 (2017).
39. Witte, J. C. et al. NASA A-Train and Terra observations of the 2010 Russian wildfires. *Atmos. Chem. Phys.* **11**, 9287–9301 (2011).
40. Hauser, M., Orth, R. & Seneviratne, S. I. Role of soil moisture versus recent climate change for the 2010 heat wave in western Russia. *Geophys. Res. Lett.* **43**, 2819–2826 (2016).
41. Chen, A. Evaluating the relationships between wildfires and drought using machine learning. *Int. J. Wildland Fire* **31**, 230–239 (2022).
42. Russo, A. et al. Assessing the role of drought events on wildfires in the Iberian Peninsula. *Agr. Forest Meteorol.* **237–238**, 50–59 (2017).
43. Silva, C. V. J. et al. Drought-induced Amazonian wildfires instigate a decadal-scale disruption of forest carbon dynamics. *Philos. T. R. Soc. B.* **373**, 20180043 (2018).
44. Bradstock, R. A., Hammill, K. A., Collins, L. & Price, O. Effects of weather, fuel and terrain on fire severity in topographically diverse landscapes of south-eastern Australia. *Landscape Ecol* **25**, 607–619 (2010).

45. Walker, X. J. et al. Fuel availability not fire weather controls boreal wildfire severity and carbon emissions. *Nat. Clim. Change* **10**, 1130–1136 (2020).
46. Abatzoglou, J. T. & Kolden, C. A. Relationships between climate and macroscale area burned in the western United States. *Int. J. Wildland Fire* **22**, 1003–1020 (2013).
47. Deb, P. et al. Causes of the widespread 2019–2020 Australian Bushfire Season. *Earth's Future* **8**, e2020EF001671 (2020).
48. Hao, Z. et al. The 2022 Sichuan-Chongqing spatio-temporally compound extremes: a bitter taste of novel hazards. *Sci. Bull.* **68**, 1337–1339 (2023).
49. Rodrigues, M., Alcasena, F. & Vega-García, C. Modeling initial attack success of wildfire suppression in Catalonia, Spain. *Sci. Total Environ.* **666**, 915–927 (2019).
50. Poulter, B., Freeborn, P. H., Jolly, W. M. & Varner, J. M. COVID-19 lockdowns drive decline in active fires in southeastern United States. *Proc. Natl Acad. Sci. USA* **118**, e2105666118 (2021).
51. Rodrigues, M., Gelabert, P. J., Ameztegui, A., Coll, L. & Vega-García, C. Has COVID-19 halted winter-spring wildfires in the Mediterranean? Insights for wildfire science under a pandemic context. *Sci. Total Environ.* **765**, 142793 (2021).
52. Sugg, M. M., Runkle, J. D., Hajnos, S. N., Green, S. & Michael, K. D. Understanding the concurrent risk of mental health and dangerous wildfire events in the COVID-19 pandemic. *Sci. Total Environ.* **806**, 150391 (2022).
53. Li, Y. et al. Vegetation net primary productivity in urban areas of China responded positively to the COVID-19 lockdown in spring 2020. *Sci. Total Environ.* **916**, 169998 (2024).
54. Su, F. et al. Rapid greening response of China's 2020 spring vegetation to COVID-19 restrictions: Implications for climate change. *Sci. Adv.* **7**, eabe8044 (2021).
55. Tang, A. C. I. et al. Detection and attribution of an anomaly in terrestrial photosynthesis in Europe during the COVID-19 lockdown. *Sci. Total Environ.* **903**, 166149 (2023).
56. Zhou, S., Zhang, Y., Park Williams, A. & Gentine, P. Projected increases in intensity, frequency, and terrestrial carbon costs of compound drought and aridity events. *Sci. Adv.* **5**, eaau5740 (2019).
57. Lian, X. et al. Seasonal biological carryover dominates northern vegetation growth. *Nat. Commun.* **12**, 983 (2021).
58. Huang, J., Yu, H., Guan, X., Wang, G. & Guo, R. Accelerated dryland expansion under climate change. *Nat. Clim. Change* **6**, 166–171 (2016).
59. Zscheischler, J. & Seneviratne, S. I. Dependence of drivers affects risks associated with compound events. *Sci. Adv.* **3**, e1700263 (2017).
60. Zheng, B. et al. Record-high CO_2 emissions from boreal fires in 2021. *Science* **379**, 912–917 (2023).
61. Qin, Y. et al. Large loss and rapid recovery of vegetation cover and aboveground biomass over forest areas in Australia during 2019–2020. *Remote Sens. Environ.* **278**, 113087 (2022).
62. Lesk, C. et al. Stronger temperature–moisture couplings exacerbate the impact of climate warming on global crop yields. *Nat. Food* **2**, 683–691 (2021).
63. Xu, S. et al. Evaluating the cumulative and time-lag effects of vegetation response to drought in Central Asia under changing environments. *J. Hydrol.* **627**, 130455 (2023).
64. Wu, D. et al. Time-lag effects of global vegetation responses to climate change. *Global Change Biol.* **21**, 3520–3531 (2015).
65. Zscheischler, J. et al. A typology of compound weather and climate events. *Nat. Rev. Earth Env.* **1**, 333–347 (2020).
66. Aragão, L. E. O. C. et al. 21st Century drought-related fires counteract the decline of Amazon deforestation carbon emissions. *Nat. Commun.* **9**, 536 (2018).
67. Bi, W. et al. A global 0.05° dataset for gross primary production of sunlit and shaded vegetation canopies from 1992 to 2020. *Sci. Data* **9**, 213 (2022).
68. Boschetti, L. et al. Global validation of the collection 6 MODIS burned area product. *Remote Sens. Environ.* **235**, 111490 (2019).
69. Giglio, L., Boschetti, L., Roy, D. P., Humber, M. L. & Justice, C. O. The Collection 6 MODIS burned area mapping algorithm and product. *Remote Sens. Environ.* **217**, 72–85 (2018).
70. Cardil, A. et al. Climate teleconnections modulate global burned area. *Nat. Commun.* **14**, 427 (2023).
71. Zhao, M., Geruo, A., Velicogna, I. & Kimball, J. S. Satellite observations of regional drought severity in the continental United States using GRACE-based terrestrial water storage changes. *J. Climate* **30**, 6297–6308 (2017).
72. Isbell, F. et al. Biodiversity increases the resistance of ecosystem productivity to climate extremes. *Nature* **526**, 574–577 (2015).
73. Hoover, D. L., Knapp, A. K. & Smith, M. D. Resistance and resilience of a grassland ecosystem to climate extremes. *Ecology* **95**, 2646–2656 (2014).
74. Li, D., Wu, S., Liu, L., Zhang, Y. & Li, S. Vulnerability of the global terrestrial ecosystems to climate change. *Global Change Biol.* **24**, 4095–4106 (2018).
75. Yao, Y., Liu, Y., Wang, Y. & Fu, B. Greater increases in China's dryland ecosystem vulnerability in drier conditions than in wetter conditions. *J. Environ. Manage.* **291**, 112689 (2021).
76. Yao, Y. et al. Evaluation of ecosystem resilience to drought based on drought intensity and recovery time. *Agr. Forest Meteorol.* **314**, 108809 (2022).
77. Yi, C. & Jackson, N. A review of measuring ecosystem resilience to disturbance. *Environ. Res. Lett.* **16**, 053008 (2021).
78. Zhang, S., Zhang, J., Liang, S., Liu, S. & Zhou, Y. A perception of the nexus "resistance, recovery, resilience" of vegetations responded to extreme precipitation pulses in arid and semi-arid regions: a case study of the Qilian Mountains Nature Reserve. *China. Sci. Total Environ.* **843**, 157105 (2022).
79. Jha, S., Das, J., Sharma, A., Hazra, B. & Goyal, M. K. Probabilistic evaluation of vegetation drought likelihood and its implications to resilience across India. *Global Planet. Change* **176**, 23–35 (2019).

Acknowledgements

This study received financial support from National Natural Science Foundation of China (42171082) and National Key R&D Program of China (2023YFC3006803). We thank Wanlu Liu from Institute of Geographic Sciences and Natural Resources Research, Chinese Academy of Sciences for help with statistical analysis. We also thank the anonymous reviewers for their fruitful comments that led to the improvement of this paper.

Author contributions

X.Z.Z. conceived and designed the project, performed most of the data analysis, interpreted the results, wrote and revised the manuscript. X.R.T. conceived and improved the project, provided ideas and supporting analyses for the analysis, interpreted the results, and contributed to the manuscript writing and revision. X.D.L. and L.F.S. interpreted the results and contributed to the manuscript revision.

Competing interests

The authors declare no competing interests.

Additional information

Supplementary information The online version contains supplementary material available at https://doi.org/10.1038/s43247-024-01406-7.

Correspondence and requests for materials should be addressed to Xiaorui Tian.

Peer review information *Communications Earth & Environment* thanks the anonymous reviewers for their contribution to the peer review of this work. Primary Handling Editors: Yongqiang Liu, Clare Davis and Aliénor Lavergne. A peer review file is available.